Coherent Phonon Heat Conduction in Superlattices

Maria N. Luckyanova *et al.*

Science **338**, 936 (2012);
DOI: 10.1126/science.1225549

17. S. Howorka, Z. Siwy, *Chem. Soc. Rev.* **38**, 2360 (2009).
18. C. Dekker, *Nat. Nanotechnol.* **2**, 209 (2007).
19. A. R. Hall *et al.*, *Nat. Nanotechnol.* **5**, 874 (2010).
20. D. Branton *et al.*, *Nat. Biotechnol.* **26**, 1146 (2008).
21. S. Majd *et al.*, *Curr. Opin. Biotechnol.* **21**, 439 (2010).
22. E. A. Manrao *et al.*, *Nat. Biotechnol.* **30**, 349 (2012).
23. N. A. W. Bell *et al.*, *Nano Lett.* **12**, 512 (2012).
24. R. Wei, T. G. Martin, U. Rant, H. Dietz, *Angew. Chem. Int. Ed.* **51**, 4864 (2012).
25. S. Burge, G. N. Parkinson, P. Hazel, A. K. Todd, S. Neidle, *Nucleic Acids Res.* **34**, 5402 (2006).
26. W. Vercoutere *et al.*, *Nat. Biotechnol.* **19**, 248 (2001).
27. A. F. Sauer-Budge, J. A. Nyamwanda, D. K. Lubensky, D. Branton, *Phys. Rev. Lett.* **90**, 238101 (2003).
28. J. Mathé, H. Visram, V. Viasnoff, Y. Rabin, A. Meller, *Biophys. J.* **87**, 3205 (2004).

Acknowledgments: Supported by the Deutsche Forschungsgemeinschaft [grant SFB 863 and Excellence Clusters NIM (Nanosystems Initiative Munich) and CIPSM (Center for Integrated Protein Science Munich)], the Bundesministerium für Bildung und Forschung (grant 13N10970), the European Research Council (starting grant GA 256270, H.D.), the Technische Universität München Institute for Advanced Study, and NIH grant 1R01GM081705 (M.M.). We thank M. Hiller and A. Bessonov for preliminary work, G. Baaken and J. Behrends for kindly providing the MECA chips, and A. Seifert, M. Beckler, and N. Fertig for technical support with the Orbit setup. M.M., H.D., and F.C.S. designed the research; M.L., V.A., and S.R. performed electrophysiological experiments; T.G.M. prepared the synthetic DNA channels and performed TEM; J.L., V.A., and T.G.M. performed experiments with lipid vesicles; and H.D. and F.C.S. wrote the paper. All authors discussed the results and commented on the manuscript.

Supplementary Materials

www.sciencemag.org/cgi/content/full/338/6109/932/DC1
Materials and Methods
Texts S1 to S9
Figs. S1 to S24
Tables S1 to S3
References (*29*–*46*)

4 June 2012; accepted 27 September 2012
10.1126/science.1225624

Coherent Phonon Heat Conduction in Superlattices

Maria N. Luckyanova,[1]* Jivtesh Garg,[1]* Keivan Esfarjani,[1] Adam Jandl,[2] Mayank T. Bulsara,[2] Aaron J. Schmidt,[3] Austin J. Minnich,[4] Shuo Chen,[5] Mildred S. Dresselhaus,[6,7] Zhifeng Ren,[5] Eugene A. Fitzgerald,[2] Gang Chen[1]†

The control of heat conduction through the manipulation of phonons as coherent waves in solids is of fundamental interest and could also be exploited in applications, but coherent heat conduction has not been experimentally confirmed. We report the experimental observation of coherent heat conduction through the use of finite-thickness superlattices with varying numbers of periods. The measured thermal conductivity increased linearly with increasing total superlattice thickness over a temperature range from 30 to 150 kelvin, which is consistent with a coherent phonon heat conduction process. First-principles and Green's function–based simulations further support this coherent transport model. Accessing the coherent heat conduction regime opens a new venue for phonon engineering for an array of applications.

Heat conduction usually occurs by a random walk of thermal energy carriers such as phonons, electrons, or molecules. During the last two decades, size effects on phonon heat conduction that lead to a deviation from this random walk behavior have drawn considerable attention (*1*). Most experimental observations of phonon size effects can be explained by invoking the Casimir picture, wherein phonons travel ballistically or quasi-ballistically through the internal region of the specimen and scatter at interfaces and boundaries (*2*). Such classical size effects are important for a wide range of applications including thermoelectric energy conversion and microelectronic thermal management.

In this classical size regime, the phase information carried by phonons is lost through the diffuse scattering of phonons at boundaries and by internal scattering processes. However, it should be possible to control the conduction of heat by manipulating phonon waves through, for example, stop-band formation in periodic structures (*3*), soliton waves (*4*), and phonon localization (*5*). Such manipulations require that heat-carrying phonons maintain their phase information throughout the heat conduction process. Coherent phonons in superlattices (SLs) have been observed with Raman and acoustic reflection and transmission experiments, but these experiments probe a single frequency (*6*–*8*), rather than the integrated distribution associated with heat transfer. Thus, a conclusive demonstration of coherent phonon heat conduction remains an open challenge.

The term "coherent" has different meanings in different fields. Typically, it is used to characterize the source of a nearly monochromatic wave and implies a measurable phase relationship for a given time interval during wave propagation. Although this definition applies to a monochromatic wave, it does not apply to heat conduction, which involves all the thermally excited phonons in a structure. To clarify the meaning of coherent heat conduction, we consider heat conduction across the thickness of a thin film. In the Casimir classical size effect regime, broadband phonons thermally excited at one boundary traverse the

[1]Department of Mechanical Engineering, Massachusetts Institute of Technology, Cambridge, MA 02139, USA. [2]Department of Materials Science and Engineering, Massachusetts Institute of Technology, Cambridge, MA 02139, USA. [3]Department of Mechanical Engineering, Boston University, Boston, MA 02215, USA. [4]Division of Engineering and Applied Science, California Institute of Technology, Pasadena, CA 91125, USA. [5]Department of Physics, Boston College, Chestnut Hill, MA 02467, USA. [6]Department of Physics, Massachusetts Institute of Technology, Cambridge, MA 02139, USA. [7]Department of Electrical Engineering and Computer Science, Massachusetts Institute of Technology, Cambridge, MA 02139, USA.

*These authors contributed equally to this work.
†To whom correspondence should be addressed. E-mail: gchen2@mit.edu

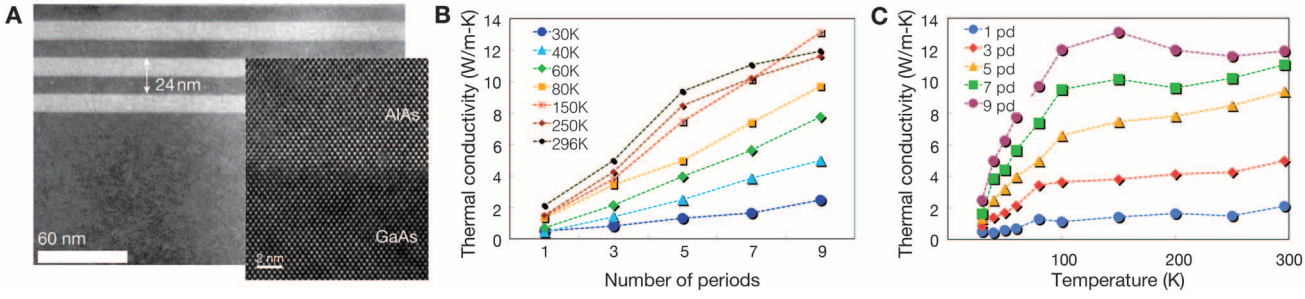

Fig. 1. (**A**) Cross-sectional TEM image of the 3-period (pd) SL. (Inset) HRTEM image of one of the interfaces. Measured thermal conductivity of GaAs/AlAs SLs as a function of (**B**) number of periods in the SL for different temperatures and (**C**) temperature for different SL thicknesses. If the interfaces in the SLs destroy the phonon coherence, the measured thermal conductivity is expected to be independent of the number of periods. Below 150 K, the linearity of the thermal conductivity versus length suggests that phonon heat conduction in these SLs is coherent.

internal region of the film ballistically. Upon reaching the sample boundary, they are usually scattered diffusely. Hence, phonon propagation inside the layer is coherent. However, because boundaries often scatter phonons diffusely, it is commonly assumed that such scattering randomizes the phases of phonons such that interference effects, and the resultant modification of the phonon dispersion, can be neglected. For a SL with many internal interfaces, the key question for heat conduction is whether each internal interface behaves as a diffuse boundary, as in the classical size effect regime, or whether it behaves as a new material with its own phonon dispersion caused by interference of phonon waves propagating through the whole structure. In the former case, phonon transport is incoherent and the SL can be thought of as a composite. In the latter case, phonon transport is coherent and the SL should be treated as one homogeneous material.

The idea of using periodic structures such as SLs and phononic crystals to control thermal transport by manipulating coherent phonons has existed for some time (*9*). Past experimental and theoretical studies, particularly those of SLs, have made such control seem unattainable except at very low temperatures (*9*, *10*). For example, in SLs, extensive experimental and theoretical studies, which have focused on changing the periodicity, have shown that interface roughness and the resulting diffuse scattering play a dominant role in the experimentally observed thermal conductivity reduction compared with their bulk parent materials (*11*–*17*), implying that phonon transport through SLs is mainly incoherent. We now show that coherent heat conduction occurs in SLs, despite the dominance of diffuse interface scattering in reducing the phonon thermal conductivity. The issue of coherent versus incoherent transport is important for understanding energy transport in a variety of disciplines.

We have taken a different experimental approach to study heat transport through SLs. Rather than changing the thickness of the SL periods, we measure the thermal transport properties of SLs with a constant period but a varying number of periods. If each internal interface scatters phonons diffusively, thus destroying their phase information, then the interface behaves like a thermal resistor because of the Kapitza resistance (*18*), such that many equivalent interfaces in series lead to an effective SL thermal conductivity, in the direction perpendicular to the interfaces, that is approximately independent of the number of layers (*15*). However, if the phase of the phonon is preserved at the interfaces of the SL and if anharmonic scattering is minimal, superposition of the Bloch waves creates stop bands and effectively modifies the phonon band structure (*10*).

In this regime, phonon mean free paths (MFPs) are equal to the sample length, leading to a thermal conductivity that is linearly proportional to the total thickness of the SL. This SL structure has the equivalent of a constant conductance through all the layers, as would be expected in a thin film with no internal scattering (*19*). In the case of a single material system, this regime is typically referred to as the "ballistic" transport regime. In the case of SLs, this implies that these phonons are eigenmodes of the SL and therefore have the modified dispersion arising from coherent wave interference effects. Therefore, in the case of SLs, ballistic transport across the whole thickness means coherent heat conduction in the SL. We should caution not to equate ballistic heat conduction to coherent heat conduction in general, because ballistic heat conduction is widely used to describe the reduced thermal conductivity of nanowires caused by diffuse scattering of phonons at the boundaries (*20*).

We used metal-organic chemical vapor deposition (MOCVD) to fabricate five GaAs/AlAs SL samples consisting of 1, 3, 5, 7, and 9 periods, where each period consists of 12 nm of GaAs and 12 nm of AlAs. Cross-sectional transmission electron microscope (TEM) images of the samples, such as Fig. 1A, were used to confirm the thickness of the layers, and high-resolution (HR) TEM images such as the inset in Fig. 1A confirmed the good quality of the interfaces between the layers. HRTEM images have low contrast for dilute concentrations of GaAs in AlAs, and vice versa, which makes determining the exact amount of interface mixing somewhat difficult. Recent

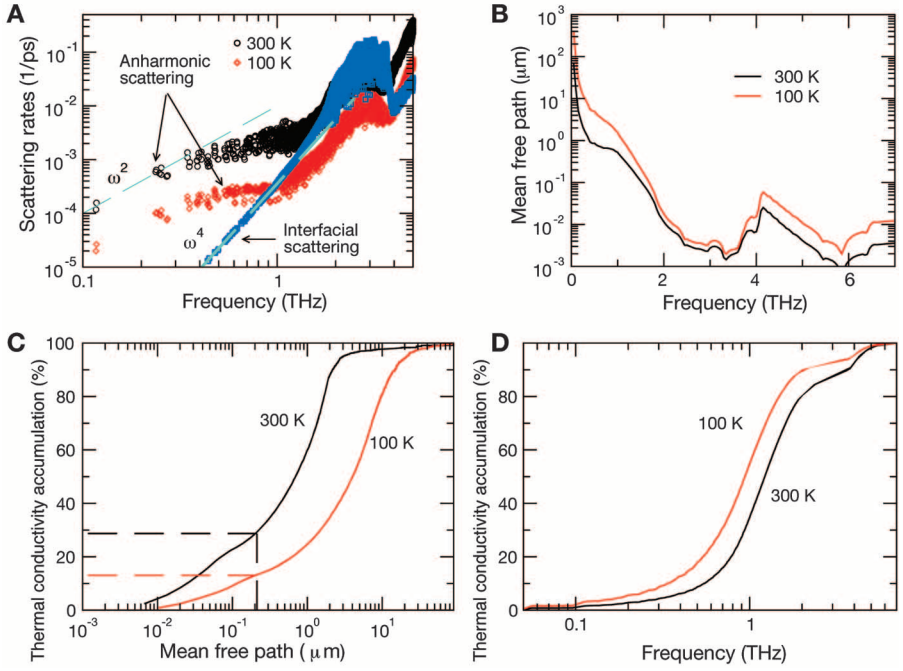

Fig. 2. Calculated first-principles results for an infinite 12 nm by 12 nm GaAs/AlAs SL. (**A**) Comparison between anharmonic (red for 100 K and black for 300 K) and interface (blue) scattering rates. Dashed blue lines are the fits to the scattering rates describing the ω^2 and ω^4 behaviors of the anharmonic and interfacial scattering, respectively, in the low-frequency regime. (**B**) Phonon MFPs in the SL as a function of frequency. Thermal conductivity accumulation in the SL as a function of (**C**) phonon MFP and (**D**) frequency, at 100 and 300 K.

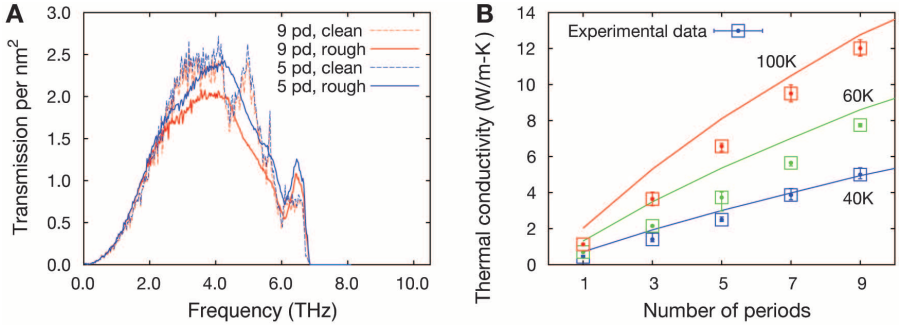

Fig. 3. (**A**) Transmission function per nm^2 of the 5- and 9-period SLs in the clean and rough boundary cases. (**B**) Thermal conductivity as a function of length at 40, 60, and 100 K for an SL with rough interfaces (solid) and experimental samples (dots with error bars).

scanning TEM (STEM) studies of GaAs/AlAs SLs grown by molecular beam epitaxy–have found interface mixing to extend over three atomic layers (*21*). The samples used in this study are expected to have slightly greater mixing due to the higher temperatures used in MOCVD.

We used time-domain thermoreflectance (TDTR) measurements to find the thermal conductivities of these samples (*13*, *22*) at temperatures between 30 and 300 K. The experiment was performed between 30 and 300 K with liquid He cooling. The TDTR experimental setup used herein was discussed in greater detail in the relevant references (*23*–*25*).

The thermal conductivities of the SL samples resulting from the TDTR experiment are given in Fig. 1, B and C. The conductivity is linear in total SL thickness from 30 to 150 K (Fig. 1B). This nearly linear dependence of thermal conductivity on number of SL periods implies coherent phonon transport through the layers, whereas the nonlinear dependence at temperatures greater than 150 K suggests the increasing influence of incoherent effects. However, because the thermal conductivity is still increasing with the period number even at 296 K, coherent phonons still conduct a considerable fraction of heat at this temperature. The effective thermal conductivities of these SLs are much smaller than that of their bulk counterparts [the room temperature thermal conductivity of GaAs is 45 W/m-K and that of AlAs is 90 W/m-K (*26*)] and are increasing with temperature.

To understand the experimental results, we used a first-principles approach based on lattice dynamics to calculate the phonon MFPs of an infinite SL at different temperatures. Unlike past theoretical approaches based on the Boltzmann transport equation (*15*), lattice dynamics (*27*, *28*), molecular dynamics (*16*, *29*, *30*), and acoustic wave equations that relied on various assumptions and fitting parameters, our first-principles approach relies on the use of harmonic and anharmonic interatomic force constants derived from density-functional perturbation theory (DFPT) (*31*) along with a solution of the Boltzmann transport equation to predict the thermal conductivity. Its use has been shown to lead to excellent agreement between experiments and theory for perfect crystals (*32*, *33*) as well as alloys (*34*). More recently, Garg *et al*. (*35*) used this approach to compute the thermal conductivity of ideal Si/Ge SLs with perfect interfaces where phonons were taken to scatter only through anharmonic processes. The computed thermal conductivity values were higher than experimental values, indicating the need to incorporate the effects of interfacial disorder.

In this work, we include both interface roughness as the random mixing of Ga and Al atoms in a narrow region around the interface and three-phonon processes from first-principles without introducing any fitting parameters. Scattering caused by this mixing was computed from Fermi's golden rule (*36*).

Based on the results of these first-principles computations, we can extract detailed information such as the phonon MFP distribution and the MFP dependence of the thermal conductivity. Although these calculations were performed for an infinite SL, the information obtained regarding phonon MFPs allowed us to gain insight into the role of coherent transport in finite-size SLs. Figure 2A shows the anharmonic and interface scattering rates at different frequencies. Although lower-frequency phonons were mostly scattered through three-phonon processes, higher-frequency phonons were also scattered by the interfacial disorder. This interfacial scattering of high-frequency phonons led to a reduction in their heat-carrying ability and caused an overall decrease in the thermal conductivity of SLs. Low-frequency phonons had long MFPs (Fig. 2B) and could propagate through the entire SL structure and thus conduct heat coherently through a SL whose thickness was shorter than the MFPs. The contribution of these long MFP phonons to the total thermal conductivity is shown in Fig. 2, C and D, where thermal conductivity accumulation is plotted against MFP and frequency, respectively. Phonons with MFPs longer than 216 nm, the thickest measured SL, contributed 87% (at 100 K) and 71% (at 300 K) to the total thermal conductivity of an infinite SL, as indicated by the dashed lines in Fig. 2C. This finding points to the important role that low-frequency, long-MFP phonons play in heat transport through the SLs. These phonons form a new band structure with altered group velocities (fig. S3) and stop bands.

Further evidence of the dominant role of coherent phonon transport in finite SLs is provided by a Green's function (GF)–based calculation of the SL thermal conductivities (*37*–*39*). This theory is purely harmonic but rigorously includes roughness effects and the finite thickness of the SLs. Because first-principles results have shown that most of the heat is conducted by low-frequency phonons that are only weakly scattered by anharmonic processes in the bulk, we expect the GF treatment, which ignores this anharmonicity, to be valid (*27*). The experimental results indicate that for the finite-thickness SLs, phonon transport was mostly coherent. In this regime, similar to the Casimir regime, the thermal conductivity of the SL was mainly determined by scattering at the sample boundaries rather than at internal interfaces.

In Fig. 3A, we show the phonon transmission function across a 5- and 9-period SL sandwiched between semi-infinite Al and GaAs leads where both clean and rough SL interfaces are considered. Low-frequency phonons were not affected by interface roughness because their wavelengths were longer than the scale of the roughness. Similarly, at low frequencies, the transmission did not vary much with sample thickness. However, high-frequency phonons had a lower transmission as the SL became longer. Figure 3B shows the thermal conductivity of the SL versus length for samples with rough interfaces. Because the transmission depended on the roughness conditions of the SL sample boundaries, which are difficult to predict due to the polycrystalline nature of the Al film, an exact match between experiments and simulation was not expected. Nevertheless, the temperature dependence of the thermal conductivity in the dominantly coherent regime (T < 100 K) was consistent between the experiments and the GF calculations. To obtain reasonable numerical agreement with experiments, the force constants between the Al layer and the SL were reduced and their masses were increased so as to artificially increase the interfacial thermal resistance by an order of magnitude. In actual experiments, it was found that this interfacial resistance depends highly on environmental and sample preparation conditions, which justifies such a treatment.

Our experimental and theoretical studies show that most of the phonons that contributed to the measured thermal conductivity in SLs traversed the SLs ballistically and hence were coherent. Interface roughness was effective in destroying the coherence of high-frequency phonons but not effective in scattering low-frequency phonons. The large reduction in thermal conductivity resulted from the loss of coherence of high-frequency phonons, but the lower-frequency phonons that contribute to the thermal conductivity were mostly coherent during their transport through the SL structures until they were scattered at the sample boundaries. This conclusion has important implications for the future of phonon engineering. For thermoelectric applications, for example, a lower thermal conductivity can be achieved if the coherence of these low-frequency phonons can be broken. The coherence of long-wavelength phonons can be destroyed by introducing perturbations that vary over long length scales. Examples of such perturbations are the strain associated with dislocations and aperiodic SLs. Indeed, some past experiments show that quantum-dot SLs (*40*), metal-dielectric SLs (*41*), and disordered, layered crystals (*42*) exhibit very low thermal conductivities that may have been the result of the destruction of long-wavelength phonon coherence. With the identification of the contribution of coherent phonons to heat conduction, we expect that strategies can be developed to further suppress or enhance the thermal conductivity of nanostructured materials.

References and Notes

1. D. G. Cahill *et al*., *J. Appl. Phys.* **93**, 793 (2003).
2. H. B. G. Casimir, *Physica* **5**, 495 (1938).
3. J.-K. Yu, S. Mitrovic, D. Tham, J. Varghese, J. R. Heath, *Nat. Nanotechnol.* **5**, 718 (2010).
4. C. W. Chang, D. Okawa, A. Majumdar, A. Zettl, *Science* **314**, 1121 (2006).
5. J. Lim, K. Hippalgaonkar, S. C. Andrews, A. Majumdar, P. Yang, *Nano Lett.* **12**, 2475 (2012).
6. C. Colvard, R. Merlin, M. V. Klein, A. C. Gossard, *Phys. Rev. Lett.* **45**, 298 (1980).
7. J. Wang *et al*., *Phys. Rev. B* **72**, 153311 (2005).
8. V. Narayanamurti, H. L. Störmer, M. A. Chin, A. C. Gossard, W. Wiegmann, *Phys. Rev. Lett.* **43**, 2012 (1979).
9. V. Narayanamurti, *Science* **213**, 717 (1981).

10. S. Tamura, D. C. Hurley, J. P. Wolfe, *Phys. Rev. B* **38**, 1427 (1988).
11. T. Yao, *Appl. Phys. Lett.* **51**, 1798 (1987).
12. X. Y. Yu, G. Chen, A. Verma, J. S. Smith, *Appl. Phys. Lett.* **67**, 3554 (1995).
13. W. S. Capinski *et al.*, *Phys. Rev. B* **59**, 8105 (1999).
14. S.-M. Lee, D. G. Cahill, R. Venkatasubramanian, *Appl. Phys. Lett.* **70**, 2957 (1997).
15. G. Chen, *Phys. Rev. B* **57**, 14958 (1998).
16. B. C. Daly, H. J. Maris, K. Imamura, S. Tamura, *Phys. Rev. B* **66**, 024301 (2002).
17. Y. K. Koh, Y. Cao, D. G. Cahill, D. Jena, *Adv. Funct. Mater.* **19**, 610 (2009).
18. E. T. Swartz, R. O. Pohl, *Rev. Mod. Phys.* **61**, 605 (1989).
19. R. Landauer, *Philos. Mag.* **21**, 863 (1970).
20. D. Li *et al.*, *Appl. Phys. Lett.* **83**, 2934 (2003).
21. P. D. Robb, A. J. Craven, *Ultramicroscopy* **109**, 61 (2008).
22. C. A. Paddock, G. L. Eesley, *J. Appl. Phys.* **60**, 285 (1986).
23. D. G. Cahill, *Rev. Sci. Instrum.* **75**, 5119 (2004).
24. A. J. Schmidt, X. Chen, G. Chen, *Rev. Sci. Instrum.* **79**, 114902 (2008).
25. Materials and methods are available as supplementary materials on *Science* Online.
26. M. A. Afromowitz, *J. Appl. Phys.* **44**, 1292 (1973).
27. P. Hyldgaard, G. D. Mahan, *Phys. Rev. B* **56**, 10754 (1997).
28. S. Tamura, Y. Tanaka, H. J. Maris, *Phys. Rev. B* **60**, 2627 (1999).
29. E. S. Landry, A. J. H. McGaughey, *Phys. Rev. B* **79**, 075316 (2009).
30. S. Volz, J. B. Saulnier, G. Chen, P. Beauchamp, *Microelectron. J.* **31**, 815 (2000).
31. S. Baroni, P. Giannozzi, A. Testa, *Phys. Rev. Lett.* **58**, 1861 (1987).
32. D. A. Broido, M. Malorny, G. Birner, N. Mingo, D. A. Stewart, *Appl. Phys. Lett.* **91**, 231922 (2007).
33. K. Esfarjani, G. Chen, H. T. Stokes, *Phys. Rev. B* **84**, 085204 (2011).
34. J. Garg, N. Bonini, B. Kozinsky, N. Marzari, *Phys. Rev. Lett.* **106**, 045901 (2011).
35. J. Garg, N. Bonini, N. Marzari, *Nano Lett.* **11**, 5135 (2011).
36. S. Tamura, *Phys. Rev. B* **27**, 858 (1983).
37. P. A. Lee, D. S. Fisher, *Phys. Rev. Lett.* **47**, 882 (1981).
38. C. Caroli, R. Combescot, P. Nozieres, D. Saint-James, *J. Phys. C Solid State Phys.* **4**, 916 (1971).
39. Y. Meir, N. S. Wingreen, *Phys. Rev. Lett.* **68**, 2512 (1992).
40. G. Pernot *et al.*, *Nat. Mater.* **9**, 491 (2010).
41. R. M. Costescu, D. G. Cahill, F. H. Fabreguette, Z. A. Sechrist, S. M. George, *Science* **303**, 989 (2004).
42. C. Chiritescu *et al.*, *Science* **315**, 351 (2007).

Acknowledgments: We thank A. A. Maznev, K. A. Nelson, K. C. Collins, and J. Johnson for helpful discussions. This material is based on work supported as part of the Solid State Solar-Thermal Energy Conversion Center (S^3TEC), an Energy Frontier Research Center funded by the U.S. Department of Energy, Office of Science, Office of Basic Energy Sciences under award DE-SC0001299/DE-FG02-09ER46577. M.N.L. was partially supported by the National Science Foundation Graduate Research Fellowship under grant 1122374.

Supplementary Materials

www.sciencemag.org/cgi/content/full/338/6109/936/DC1
Materials and Methods
Figs. S1 to S4
References (*43*–*57*)

4 June 2012; accepted 9 October 2012
10.1126/science.1225549

Evidence for a Dynamo in the Main Group Pallasite Parent Body

John A. Tarduno,[1,2]* Rory D. Cottrell,[1] Francis Nimmo,[3] Julianna Hopkins,[2] Julia Voronov,[1] Austen Erickson,[1,2] Eric Blackman,[2] Edward R.D. Scott,[4] Robert McKinley[1]

Understanding the origin of pallasites, stony-iron meteorites made mainly of olivine crystals and FeNi metal, has been a vexing problem since their discovery. Here, we show that pallasite olivines host minute magnetic inclusions that have favorable magnetic recording properties. Our paleointensity measurements indicate strong paleomagnetic fields, suggesting dynamo action in the pallasite parent body. We use these data and thermal modeling to suggest that some pallasites formed when liquid FeNi from the core of an impactor was injected as dikes into the shallow mantle of a ~200-kilometer-radius protoplanet. The protoplanet remained intact for at least several tens of millions of years after the olivine-metal mixing event.

Lord Rayleigh (Robert John Strutt) (*1*) noted the paradox posed by pallasite meteorites: Olivine and metal seemingly should have separated into layers in their parent body. Some models, to avoid segregation, have invoked small metal pools throughout a parent body (*2*), but the putative scenario has remained in formation near a core-mantle boundary (*3*). There are ~50 known pallasite meteorites. Most have isotopic ratios that fall near the terrestrial mass fractionation line and are called "main group" pallasites (*4*). Olivine ranges from Fa_{11} to Fa_{20} and often occurs as centimeter-sized (Fig. 1, A and B) crystals (*5*–*8*), with a dislocation density (*9*) comparable with those of unshocked terrestrial samples. The metal in main group pallasites is Ir poor and is thought to have originated from the residual melt fraction of a core similar in composition to IIIAB iron meteorites (*3*).

Paleomagnetism might help to distinguish between models for pallasite formation, but prior attempts have failed to yield interpretable data. The massive FeNi of the pallasite matrix is the likely culprit. This metal is similar to that composing iron meteorites, which carries a highly anisotropic, soft magnetization; it is notoriously poor as a paleomagnetic recorder (*10*, *11*). Paleomagnetic studies of other meteorites [for example, (*12*–*13*)], however, suggest some parent bodies hosted dynamos. Modeling suggests bodies >80 km in radius could be in the regime of supercritical magnetic Reynolds numbers, in which large-scale dynamo action is possible (*14*, *15*).

Rather than studying bulk material, we applied techniques of single-silicate crystal analysis (*16*, *17*) to an investigation of the Imilac and Esquel main group pallasites. We selected gem-like olivine subsamples ≳0.5 cm from the meteorite edge and several millimeters from the olivine/metal contact. Prior studies (*18*, *19*) suggest that at these distances, heating effects due to atmospheric entry are negligible.

We have observed strings of large inclusions, tens of micrometers in size (Fig. 1C), in some olivines using transmitted light microscopy. Scanning electron microscopy (SEM) reveals isolated and strings of much smaller inclusions (≲10 μm) (Fig. 1D) that are composed of Fe, Ni, S, and Cr (fig S3). Microprobe analyses detail submicrometer-sized, irregularly spaced FeNi particles within these smaller inclusions, surrounded by troilite (fig S4). These metal particles are sometimes Ni rich [~51 to 58 weight percent (wt %) Ni] and are potential stable magnetic recorders.

Olivine subsamples lacking inclusions visible to the naked eye show pseudo-single– to single-domain magnetic hysteresis behavior (Fig. 1, E and F). In contrast, samples with visible inclusions have multidomain behavior. In the former case, we find only a slight anisotropy (Fig. 1G), and first-order reversal curves (*20*) fail to show substantial magnetic interactions (Fig. 1H). Thus, we further selected olivine subsamples lacking visible inclusions because they can have optimal properties for paleointensity determination (*21*).

Many meteorites have been exposed to magnetic contamination during collection (*13*). We therefore first used alternating field demagnetization, which revealed removal of magnetizations after the application of low peak fields (5 to 10 mT). Magnetization directions stabilized after this pretreatment, and it was here that we started thermal demagnetization. We used thermal methods because they best replicate the potential magnetization acquisition process [thermoremanent magnetization (TRM)] (*21*). In many meteorites, magnetic mineral alteration accompanying thermal treatment is severe (*11*–*13*). Studies of terrestrial samples indicate that inclusions in single-silicate crystals are less susceptible to alteration (*16*, *17*).

[1]Department of Earth and Environmental Sciences, University of Rochester, Rochester, NY 14627, USA. [2]Department of Physics and Astronomy, University of Rochester, Rochester, NY 14627, USA. [3]Department of Earth and Planetary Sciences, University of California, Santa Cruz, CA 95064, USA. [4]Hawaii Institute for Geophysics and Planetology, University of Hawaii, Manoa, HI 96822, USA.

*To whom correspondence should be addressed. E-mail: john.tarduno@rochester.edu